Nuclear Physics A556 (1993) 601–620
North-Holland

NUCLEAR
PHYSICS A

# Maximum asymmetry phenomena in $\bar{p}p \to \pi^- \pi^+$ and $\bar{p}p \to K^- K^+$ reactions

Sachiko Takeuchi,[1] Fred Myhrer and Kuniharu Kubodera
*Department of Physics and Astronomy, University of South Carolina, Columbia, SC 29208, USA*

Received 2 December 1992

**Abstract:** We present an illustrative analysis to show that a simple relation between the helicity-flip and helicity-nonflip partial-wave amplitudes can account for the strikingly large asymmetries observed in the $\bar{p}p \to \pi^- \pi^+$ and $\bar{p}p \to K^- K^+$ reactions. Our study supports the argument that the final $K^- K^+$ state originates from a more central reaction than the $\pi^- \pi^+$ final state. The rather general nature of our approach leads to the expectation that the large asymmetries are likely to persist at higher energies until the perturbative QCD regime sets in.

## 1. Introduction

The differential cross sections and the asymmetries $A_{0n}$ of the two annihilation reactions $\bar{p}p \to \pi^- \pi^+$ and $\bar{p}p \to K^- K^+$ were measured at several values of the antiproton momentum up to $p_{lab} = 2.2$ GeV/$c$ [refs. [1,2])]. These experimental results have been confirmed by recent LEAR and KEK experiments [3,4]). The asymmetries $A_{0n}$ observed for the highest LEAR energies exhibit extremely noteworthy features. The reaction $\bar{p}p \to \pi^- \pi^+$ has very large values for $A_{0n}$ over a wide angular region for $p_{lab} \gtrsim 1.5$ GeV/$c$. Even more strikingly, $A_{0n}$ for the reaction $\bar{p}p \to K^- K^+$ stays close to $+1$, its maximum possible value, in a very wide angular region for $p_{lab} \gtrsim 1$ GeV/$c$. The angular shapes of these $A_{0n}$ appear to be almost independent of $p_{lab}$ at these high LEAR energies. This angular behavior of $A_{0n}$ is in marked contrast to the observed strong angular variation of the differential cross section: the $d\sigma/d\Omega$ for the final $\pi^- \pi^+$ reaction shows pronounced angular oscillations whereas $d\sigma/d\Omega$ of the final $K^- K^+$ reaction has a strong forward peak and a smooth backward "plateau". The shape of $d\sigma/d\Omega$ for either case depends only weakly on the incident antiproton momentum for $p_{lab} > 1.5$ GeV/$c$.

From a subnucleonic viewpoint, the $\bar{p}p \to \pi^- \pi^+$ and $\bar{p}p \to K^- K^+$ reactions can be significantly different in nature, since $\bar{p}p \to K^- K^+$ involves the annihilation of two

Correspondence to: Prof. S. Takeuchi, Department of Physics, Faculty of Science, Tokyo Institute of Technology, Ohokayama, Meguro, Tokyo 152, Japan.

[1] Present address: Department of Physics, Tokyo Institute of Technology, Ohokayama, Meguro, Tokyo 152, Japan.

initial $\bar{q}q$-pairs accompanied by the creation of an $\bar{s}s$-pair, while $\bar{p}p \to \pi^-\pi^+$ can occur simply by annihilating one $\bar{q}q$-pair (fig. 1). On the other hand, in an effective meson-baryon theory, these two reactions are expected to be similar to each other since they both involve two pseudo-scalar mesons in the final state. What kind of reaction mechanism is more adequate can depend on the incident energy. The data [2-4]) on the angular dependence of $A_{0n}$ and $d\sigma/d\Omega$ of the $\bar{p}p \to \pi^-\pi^+$ and $\bar{p}p \to K^-K^+$ reactions seem to suggest three energy regions corresponding to different pictures. At sufficiently high energies ($p_{lab} >$ several GeV/$c$), a perturbative QCD treatment of these reactions is expected to be relevant. At low energies ($p_{lab} \lesssim$ 1 GeV/$c$) the coupling of the appropriate hadronic channels seems to offer a natural description of the reaction mechanism; applications of the coupled-channels method are reported in refs. [5,6]), see also Mundigl *et al.* [7]). As the incident energy goes above ~1 GeV/$c$, however, the meaning and practicality of the explicit enumeration of all participating hadron channels diminish quickly; by the time one reaches the higher LEAR energies ($p_{lab} \approx 1.5$ GeV/$c$) the usefulness of the effective coupled-channels approach should be questioned. Meanwhile, one generally expects that the LEAR energy region is still below the energy regime where perturbative QCD is valid. Thus, the energy region in which the aforementioned large asymmetries arise lies between the low-energy regime dominated by a limited number of effective hadronic channels and the high-energy regime characterized by the quark-gluon degrees of freedom.

An early model analysis of the $\bar{p}p \to \pi^-\pi^+$ reaction measurements in the LEAR high-energy region introduced meson resonances with spins $J = 3$, 4 and 5 at $E_{c.m.} = 2150$, 2310 and 2480 MeV, respectively, to account for the behavior of the differential cross sections [8]). The presence of these resonances were inferred by analyzing Barrelet zeros of the complex partial-wave amplitudes [8]) under the drastic assumption that only one of the partial waves dominates at each energy. This type of analysis has been criticized by several authors [9,10]). A recent partial-wave analysis based on dispersion relation theory of the $\bar{p}p \to \pi^-\pi^+$ reaction [11]) is not incompatible with "resonance activity" in some partial-wave amplitudes, and there is the possibil-

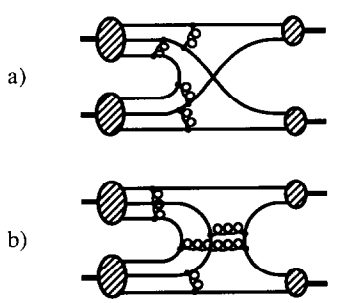


Fig. 1. Typical graphs for (a) $\bar{p}p \to \pi^-\pi^+$ and (b) $\bar{p}p \to K^-K^+$ reactions.

ity that these "resonances" correspond to some of the many excited mesons predicted by constituent quark models [12]). However, the dispersion approach cannot be readily applied to the $\bar{p}p \to K^- K^+$ reaction, since available data on the corresponding crossed channel reaction is at present very limited.

In this article we propose an alternative phenomenological description which does not require any explicit meson resonances, and which can reproduce in a natural manner the observed behavior of $A_{0n}$ and $d\sigma/d\Omega$ in the higher LEAR energy region for both the $\bar{p}p \to \pi^- \pi^+$ and $\bar{p}p \to K^- K^+$ reactions*. Although our approach is phenomenological, we argue that there exists some intuitive justification of its basic ingredients. The fact that $J/p_{c.m.}$'s for the resonances that appear in the above-mentioned analysis are approximately constant ($\approx 1.1 \sim 1.2$ fm) seems to suggest that a geometrical treatment can be a more suitable approach to these reactions.

In sect. 2, we present schematic models to illustrate that a simple assumption relating the helicity-flip and helicity-nonflip amplitudes [eq. (5)] can lead to smooth angular and energy dependences of $A_{0n}$ while giving considerable angular oscillations in the differential cross sections. In addition to the basic ansatz expressed in eq. (5), these schematic models are based on two key features of the reactions: (1) extremely strong absorption in the incident channel and (2) strong final-state interactions. The parameters characterizing these key features are treated as adjustable parameters, but the relative values of these parameters determined by fitting the data will be found to have rather simple physical interpretations. In particular, the values of these parameters indicate that the $\bar{K}K$ final state originates from a shorter-distance process than the $\pi\pi$ final state as suggested in ref. [15]).

We present in sect. 3 a somewhat more dynamical model based on a DWBA-type calculation and discuss to what extent this DWBA-type calculation supports the basic assumptions used in the schematic models of sect. 2. (We must warn the reader that our "dynamical" model is still not much more than a toy model and falls far short of a full-fledged dynamical calculation.)

Sect. 4 is devoted to a summary of the main aspects learned from the present illustrative treatments and to a brief description of the expected behavior of $A_{0n}$ as the incident energy reaches the SuperLEAR and KAON energy region.

## 2. Schematic models

### 2.1. BASIC ANSATZ

Each of the reactions under consideration can be characterized by two independent helicity amplitudes: $f_{++}$ (helicity nonflip) and $f_{+-}$ (helicity flip). In terms of these two amplitudes the differential cross section $d\sigma/d\Omega$ and the asymmetry $A_{0n}$ are

* A part of the current work was briefly reported in refs. [13,14]).

given as

$$\frac{d\sigma}{d\Omega} = |f_{++}|^2 + |f_{+-}|^2 , \tag{1}$$

$$A_{0n} = 2\,\mathrm{Im}\,(f_{++}^* f_{+-})/(d\sigma/d\Omega) . \tag{2}$$

The amplitudes $f_{++}$ and $f_{+-}$ can be expanded in terms of the partial-wave amplitudes, $T_+^J$ and $T_-^J$:

$$f_{++} = \frac{1}{p} \sum_{J=0}^{\infty} (J+\tfrac{1}{2}) T_+^J(p) P_J(\cos\theta) , \tag{3}$$

$$f_{+-} = \frac{1}{p} \sum_{J=1}^{\infty} \frac{J+\frac{1}{2}}{\sqrt{J(J+1)}} T_-^J(p) P_J'(\cos\theta) \sin\theta , \tag{4}$$

where $p$ is the $\bar{p}p$ relative momentum in the center-of-mass system. The conservation of parity and angular momentum implies that only tensor-coupled $\bar{N}N$ partial waves ($J = L \pm 1$) contribute to this reaction.

The basic ansatz of this work is that $T_-^J$ is given by the derivative of $T_+^J$ with respect to $b$, the impact parameter*:

$$T_-^J \propto \frac{\partial T_+^J}{\partial b} . \tag{5}$$

Since this ansatz presupposes a semiclassical regime where the impact parameter has a physical meaning, we may use a semiclassical relation $J \sim pb$ to rewrite eq. (5) as a relation between the partial-wave amplitudes:

$$T_-^J \propto \Delta T_+^J / \Delta J \tag{6}$$

or more specifically

$$\frac{J+\frac{1}{2}}{\sqrt{J(J+1)}} T_-^J = \frac{1}{2\beta} (T_+^{J+1} - T_+^{J-1}) , \tag{7}$$

where $\beta$ is a parameter which is allowed to depend on the momentum $p$ but not on $\theta$ or on $J$. Eq. (7) is the discretized version of our ansatz, eq. (5), and we shall refer to eq. (7) as the "basic difference equation". Note that the factor $(J+\frac{1}{2})/\sqrt{J(J+1)} \sim 1$ when the semiclassical relation $J \sim pb$ is a reasonable approximation.

In the subsequent subsections, we shall illustrate how our basic ansatz eq. (5) or its discretized variant eq. (7) leads to a smooth angular dependence of $A_{0n}$.

* A similar relation in this momentum range has been found phenomenologically in the corresponding $t$-channel process, $\pi N$ scattering [16]), as well as in $\bar{p}p$ elastic scattering [17]).

### 2.2. A SIMPLE MODEL BASED ON THE DIFFRACTION MODEL

Our first example is a highly schematic model motivated by the diffraction model for forward scattering. Assume that the helicity-conserving partial-wave amplitude is given by

$$T_+^J = iA\Theta(pR - pb)\,, \tag{8}$$

where $A$ is a constant, $\Theta$ is the step function, and $R$ stands for the range of the interaction region. Our basic assumption, eq. (5), implies that the helicity-flip partial-wave amplitude is given by

$$T_-^J = -B\delta(pR - pb)\,, \tag{9}$$

where $B$ is another constant. Thus $T_-^J$ is only operative on the surface of the interaction region. For forward scattering, i.e., $\theta \ll 1$, and for $J \sim pb \sim 1/\theta \gg 1$, we have $P_J(\cos\theta) \sim J_0(pb \sin\theta)$. Then, by replacing the summation over $J$ in eqs. (3) and (4) with the integration over $pb$, we obtain

$$f_{++} = \frac{iA}{p}\int_0^\infty \mathrm{d}(pb)\, pbJ_0(pb\sin\theta)\Theta(pR - pb) \tag{10}$$

$$= iAR\frac{J_1(pR\sin\theta)}{\sin\theta}\,, \tag{11}$$

$$f_{+-} = -\frac{B}{p}\int_0^\infty \mathrm{d}(pb)\, pbJ_1(pb\sin\theta)\delta(pR - pb) \tag{12}$$

$$= -BRJ_1(pR\sin\theta)\,. \tag{13}$$

Thus this simple illustrative model gives for forward angles

$$A_{0n} \sim 2AB\frac{\sin\theta}{A^2 + B^2\sin^2\theta}\,, \tag{14}$$

Note that this specific analytic discussion is based on the forward-scattering approximation and cannot be used to discuss the complete angular dependence of $A_{0n}$. Let us emphasize, however, the two important features which may remain in the subsequent more general cases. Namely, $A_{0n}$ of eq. (14) has no explicit energy dependence, and the range $R$ of the interaction region does not appear explicitly.

### 2.3. MORE GENERAL CONSIDERATIONS

We now study more general consequences of the ansatz eq. (5) or eq. (7) without invoking the extreme forward-scattering approximation so that we can study the general angle dependence. To this end, we start with the basic difference equation,

eq. (7), and substitute eq. (7) into eqs. (3) and (4). The use of the identity $(2J+1)P_J = P'_{J+1} - P'_{J-1}$ leads to

$$f_{+-} = -\frac{1}{\beta} f_{++} \sin\theta . \tag{15}$$

Eq. (2) then gives the asymmetry

$$A_{0n} = \frac{2\,\mathrm{Im}\,\beta \sin\theta}{|\beta|^2 + \sin^2\theta} , \tag{16}$$

which is capable of having a smooth angular dependence. For example, with a pure imaginary $\beta(=i)$, $A_{0n}$ of eq. (16) will be larger than 0.9 over a very wide angular range ($|\cos\theta| \lesssim 0.8$). On the other hand, the differential cross section

$$\mathrm{d}\sigma/\mathrm{d}\Omega = \left|\frac{f_{++}}{\beta}\right|^2 (|\beta|^2 + \sin^2\theta) \tag{17}$$

may have a significantly stronger angular dependence due to $f_{++}(\theta)$. Thus, to the extent that $\beta$ depends only weakly on the incident energy, we have succeeded in explaining the salient features of the observed $A_{0n}$ and $\mathrm{d}\sigma/\mathrm{d}\Omega$ mentioned in the introduction. We shall show below (in this section) that with physically reasonable assumptions one can construct a model in which $\beta$ is either independent of or only weakly dependent on the incident energy.

It should be remarked that essentially the same argument applies to any reactions that have similar spin kinematics and that are characterized by large angle-independent asymmetries and oscillatory differential cross sections.

From eqs. (16) and (17) we see that the parameter $\beta$ appearing in the basic difference equation, eq. (7), determines the angular shape of $A_{0n}$ and the differential cross section. We now construct specific examples of scattering amplitudes in which the value of $\beta$ is such that $A_{0n} \sim 1$ indeed holds for substantial ranges of $\theta$ *and* $p_{\mathrm{lab}}$.

We first observe that at these energies there is a strong $\bar{\mathrm{N}}\mathrm{N}$ absorption in the low impact-parameter region so that the $\bar{\mathrm{N}}\mathrm{N}$ partial-wave amplitudes with low $L$ ($L=$ orbital angular momentum for $\bar{\mathrm{N}}\mathrm{N}$ channel) approach their unitarity limit. Furthermore, the two final-state pseudoscalar mesons interact with each other in all the relevant partial waves. They are also coupled to many open meson channels, which greatly suppress the flux going into the observed final two meson states. We therefore assume that the helicity nonflip partial-wave amplitudes are given by "classical" gray- or black-sphere amplitudes: viz,

$$T_+^J = \begin{cases} B \exp[-aJ] & J \lesssim J_{\max} \\ 0 & J > J_{\max} , \end{cases} \tag{18}$$

where $B$ and $a$ are constants. The amplitude $T_-^J$ is obtained using the basic difference equation, eq. (7).

TABLE 1

Favored values of the parameters in the diffraction model

| | $a$ | $\beta$ | $J_{max}$ |
|---|---|---|---|
| $\bar{p}p \to \pi^-\pi^+$ | 0 | $i$ | 4 |
| $\bar{p}p \to K^-K^+$ | 0.5 | $i$ | $\geq 4$ |

Now we can place constraints on $\beta$ and $a$ by demanding that the observed structure of $d\sigma/d\Omega$ and $A_{0n}$ be reproduced reasonably well. Since the highest LEAR energy is most favorable for the diffraction model, we consider the data for $p_{lab} \approx 1.5$ GeV/$c$ as an example. The values of $\beta$ and $a$ favored by this condition are listed in table 1. (We use here the word "favored" instead of "optimized" to emphasize that we have only carried out an approximate parameter search.) The cross section and asymmetry obtained with these favored parameters are shown in fig. 2. These results indicate that the basic difference equation for the partial-wave amplitude, eq. (7), can indeed lead to $A_{0n} \sim 1$ over a wide angular range, giving at the same time strongly angular-dependent differential cross sections.

The amplitude for the $\bar{p}p \to \pi^-\pi^+$ reaction with $a = 0$ corresponds to a "black sphere" amplitude, whereas the $\bar{p}p \to K^-K^+$ amplitude with $a > 0$ corresponds to that of a "gray sphere" amplitude; the radii of the spheres are approximately given by $J_{max}/p$ ($\sim 1.3$ fm). Our numerical results indicate that the main contributions to the $\bar{p}p \to K^-K^+$ reaction come from the two lowest partial waves ($L = 0, 1$). The results for $\bar{p}p \to K^-K^+$ are essentially independent of $J_{max}$ as long as $J_{max} \geq 4$, whereas the $\bar{p}p \to \pi^-\pi^+$ reaction involves all $L = 0 \sim 4$ partial waves. In other words, the favored values of $a$ and $J_{max}$ given in table 1 suggest that the $\bar{p}p \to \pi^-\pi^+$ reaction requires a larger reaction volume than the $\bar{p}p \to K^-K^+$. This feature is in accordance with the argument of Carbonell *et al.* [15]), who examined the QED "annihilation"

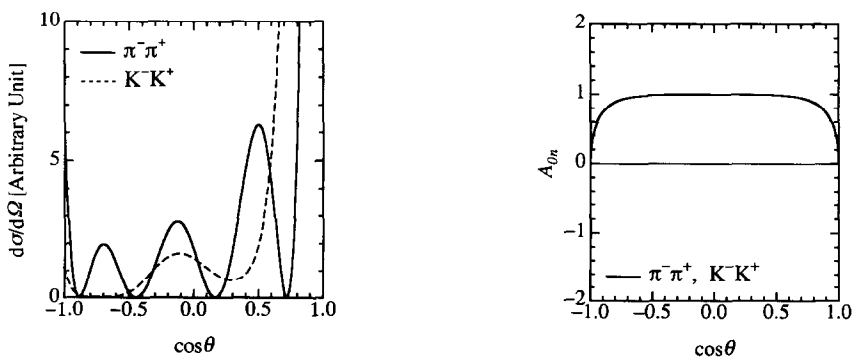


Fig. 2. (a) Differential cross sections $d\sigma/d\Omega$ and (b) asymmetries $A_{0n}$ calculated with the simple diffraction amplitude eq. (18). In (a), the solid line is for the $\bar{p}p \to \pi^-\pi^+$ reaction while the dashed line is for the $\bar{p}p \to K^-K^+$ reaction. In (b), the results for the two reactions are indistinguishable.

channels for a muonium ($\mu^+e^-$) interacting with an antimuonium ($\mu^-e^+$). According to these authors, the final state $(\mu^+\mu^-)+(e^+e^-)$, which is a rearrangement process requiring only the overlap of the atomic systems, is a more peripheral collision than the atomic collision leading to the "annihilation" channel $(\mu^+\mu^-)+\gamma$ (or $e^+e^-+\gamma$), where one pair of initial leptons is annihilated. The reason is that the $e^+e^-\to\gamma$ (or $\mu^+\mu^-\to\gamma$) reaction is pointlike. This argument suggests that the third possible "annihilation" reaction with a $\gamma\gamma$ final state should arise from a very central collision between the two initial atomic systems, since all the initial leptons are annihilated. Carbonell *et al.* pointed out that an analogous picture should also hold for the $\bar{p}p$ annihilation reactions, hadrons being composite particles made of valence quarks. The application of this picture to the present cases leads to the following expectation. Since the number of valence quark pairs to be created/annihilated is (on the average) larger in $\bar{p}p\to K^-K^+$ than in $\bar{p}p\to\pi^-\pi^+$, one expects $\bar{p}p\to K^-K^+$ to occur for more central $\bar{N}N$ collisions than the $\bar{p}p\to\pi^-\pi^+$ reaction. Although it is unlikely that reactions at $p_{\rm lab}\sim 1.5$ GeV/$c$ is fully describable in the perturbative QCD picture, the qualitative feature of the competition between the central and more peripheral processes may remain valid even in this low-energy region.

It should be noted that the shape of $A_{0n}$ does not reflect the size of the reaction volume insofar as eq. (7) holds. The asymmetries $A_{0n}$ are the same for both the $\bar{p}p\to K^-K^+$ and the $\bar{p}p\to\pi^-\pi^+$ reactions even though the angular shapes of $d\sigma/d\Omega$ for the two reactions differ significantly. Let us recall that this feature was also seen in the previous example based on the forward-scattering approximation.

## 3. A DWBA-type approach

In the preceding section we showed that our basic ansatz eq. (5) or eq. (7) could lead to a reasonable explanation of the observed behavior of $A_{0n}$ and $d\sigma/d\Omega$. To shed some light on what kind of reaction mechanism can give rise to a relation like eq. (5) or eq. (7), we shall perform a simplified DWBA-type calculation. In the usual DWBA, the $T$-matrix has the form:

$$\langle \boldsymbol{k}_f|T|\boldsymbol{k}_i SS_z\rangle = \langle\!\langle \boldsymbol{k}_f|T^{\rm tr}|\boldsymbol{k}_i SS_z\rangle\!\rangle\,, \tag{19}$$

where $|\,\rangle\!\rangle$ stands for a distorted wave function, $\boldsymbol{k}_i$ and $\boldsymbol{k}_f$ are the initial and final momenta, respectively, and $T^{\rm tr}$ is the transition operator which changes a $\bar{N}N$ state into a two-meson state; $S(=1)$ is the spin of the $\bar{N}N$ state and $S_z$ its $z$-component. Since the final-state interaction is not well known at these energies, we consider an operator $\Gamma$ that represents the combined effects of $T^{\rm tr}$ and the final-state interaction,

$$\langle \boldsymbol{k}_f|T|\boldsymbol{k}_i SS_z\rangle = \langle \boldsymbol{k}_f|\Gamma|\boldsymbol{k}_i SS_z\rangle\!\rangle\,. \tag{20}$$

We call $\Gamma$ the effective transition operator and assume that $\Gamma$ has a simple form

$$\Gamma = \left\{ V_p(r,E)\frac{1}{i}\boldsymbol{p} + V_r(r,E)\boldsymbol{r}\right\}\cdot\boldsymbol{\Sigma}^{\rm trans}\,, \tag{21}$$

where $\boldsymbol{p} = \nabla/i$ and $\boldsymbol{\Sigma}^{\text{trans}}$ is the transition-spin operator defined by the reduced matrix element $\langle 0 \| \boldsymbol{\Sigma}^{\text{trans}} \| 1 \rangle = \sqrt{6}i$. The coefficients $V_p$ and $V_r$ will be rather loosely referred to as transition potentials. If we neglect, for simplicity, possible angular dependences in the transition potentials, then the $T$-matrix can be written schematically as:

$$\langle T \rangle = \sum_{j=1}^{3} \Lambda_j \langle 00 | \Sigma_j^{\text{trans}} | SS_z \rangle, \tag{22}$$

where the $j$th component of the vector $\boldsymbol{\Lambda}$ is defined by:

$$\Lambda_j = \langle \boldsymbol{k}_f | \left[ V_p(r, E) \frac{1}{i} \boldsymbol{p} + V_r(r, E) \boldsymbol{r} \right]_j | \boldsymbol{k}_i \rangle\!\rangle \tag{23}$$

$$\equiv i\tilde{\alpha}(k_i^2, k_f^2, \cos\theta)[\{\tilde{\beta}(k_i^2, k_f^2, \cos\theta) - \cos\theta\}\hat{\boldsymbol{k}}_i + \hat{\boldsymbol{k}}_f]_j . \tag{24}$$

Here $\theta$ is the angle between $\boldsymbol{k}_i$ and $\boldsymbol{k}_f$, and $\hat{\boldsymbol{k}}_i$ ($\hat{\boldsymbol{k}}_f$) is the unit vector in the direction of $\boldsymbol{k}_i$ ($\boldsymbol{k}_f$).

The helicity amplitudes for the annihilation reaction $\bar{p}p \to M^- M^+$ corresponding to the matrix elements between nonrelativistic wave functions are given as

$$f_{++} = \tfrac{1}{2} C \langle M^- M^+; \boldsymbol{k}_f | \Gamma | \bar{p}p; \boldsymbol{k}_i S = 1, S_z = 0 \rangle\!\rangle , \tag{25}$$

$$f_{+-} = \sqrt{\tfrac{1}{2}} C \langle M^- M^+; \boldsymbol{k}_f | \Gamma | \bar{p}p; \boldsymbol{k}_i S = 1, S_z = 1 \rangle\!\rangle \tag{26}$$

with

$$C^2 = (2\pi)^4 \frac{4\rho_f \rho_i}{k_i^2}, \tag{27}$$

where $\rho_f$ ($\rho_i$) is the energy state density for the final (initial) state: $\rho \equiv \partial E/\partial k$. By choosing the $z$-axis along $\boldsymbol{k}_i$ we obtain

$$f_{++} = \frac{C}{2} \frac{\sqrt{2}}{i} \Lambda_z = \sqrt{\tfrac{1}{2}} C \tilde{\alpha} \tilde{\beta} \tag{28}$$

$$f_{+-} = i\sqrt{\tfrac{1}{2}} C (\Lambda_x + i\Lambda_y) = -\sqrt{\tfrac{1}{2}} C \tilde{\alpha} \sin\theta \, e^{i\phi} . \tag{29}$$

This leads to the asymmetry

$$A_{0n} = \frac{2 \operatorname{Im} \tilde{\beta} \sin\theta}{|\tilde{\beta}|^2 + \sin^2\theta} \tag{30}$$

and the cross section

$$\frac{d\sigma}{d\Omega} = \tfrac{1}{2} C^2 |\tilde{\alpha}|^2 \{|\tilde{\beta}|^2 + \sin^2\theta\} , \tag{31}$$

which should be compared with eqs. (16) and (17). Note that in the earlier argument in sect. 2, which was meant to illustrate typical consequences of a simple diffraction model, $\beta$ of eq. (7) was independent of $\theta$. Here, we take both $\tilde{\alpha}$ and $\tilde{\beta}$ of eq. (24) to be functions of $k_i$, $k_f$ and $\theta$ in order to see whether the values of $\tilde{\beta}$ determined from the data have actually no strong angular dependence.

To proceed with our DWBA-type calculation, we now specify the transition potentials $V_p(r, E)$ and $V_r(r, E)$ in eq. (21). We choose $V_r$ to be a sum of gaussians:

$$V_r(r, E) = \sum_{i=1}^{2} V_i(E)\, e^{i\theta_i(E)} \exp\left[-\left(\frac{r-R_i}{a_i}\right)^2\right], \tag{32}$$

where $R_i$, $a_i$, $V_i(E)$ and the phase angles $\theta_i(E)$ are parameters. In order to specify $V_p$, we find it convenient to introduce the Fourier transforms of the transition potentials. So we define

$$\tilde{V}_{r[p]}(q) \equiv \int \mathrm{d}\boldsymbol{r}\, e^{-i\boldsymbol{q}\cdot\boldsymbol{r}} V_{r[p]}(r) \tag{33}$$

with $\boldsymbol{q} \equiv \boldsymbol{k}_f - \boldsymbol{k}_i$. We have already defined $V_r(r)$ in eq. (32) so that $\tilde{V}_r(q)$ is known. Meanwhile, we choose to determine $V_p(r)$ by giving $\tilde{V}_p(q)$. In fact, we give $\tilde{V}_p(q)$ by specifying the ratio

$$c(q) \equiv -\frac{(\mathrm{d}/(q\,\mathrm{d}q))\tilde{V}_r(q)}{\tilde{V}_p(q)} \tag{34}$$

rather than $\tilde{V}_p(q)$ itself. The reason is that, as will be discussed below [cf. eq. (37)], $c(q)$ is directly related to $\tilde{\beta}$, which determines $A_{0n}$ through eq. (30). In this work $c(q)$ is assumed to have the following restricted form:

$$c(q) = c_0 + c_1 \frac{q^2}{2k_i^2}, \tag{35}$$

where $c_0 \equiv |c_0|\, e^{i\phi_0}$ and $c_1 \equiv |c_1|\, e^{i\phi_1}$ are complex parameters. These parameters along with $R_i$, $a_i$, $V_i(E)$ and $\theta_i(E)$ in eq. (32) will be determined through a fit to data.

To illustrate how the amplitudes $f_{++}$ and $f_{+-}$ and the observables depend on the transition potentials, we first use the plane-wave approximation (PWBA). This simplification allows us to derive transparent relations between $\tilde{V}_r$, $\tilde{V}_p$ on one hand and $\tilde{\alpha}$, $\tilde{\beta}$ on the other:

$$\tilde{\alpha} = \frac{i}{(2\pi)^3} \frac{\mathrm{d}}{q\,\mathrm{d}q} \tilde{V}_r(q), \tag{36}$$

$$\tilde{\beta} = \cos\theta - \frac{k_i}{k_f}(1 - c(q)), \tag{37}$$

which means $\tilde{\beta}$ has the form

$$\tilde{\beta} = \frac{k_i}{k_f}\left(c_0 - 1 + c_1 \frac{k_i^2 + k_f^2}{2k_i^2}\right) + (1 - c_1)\cos\theta. \tag{38}$$

This PWBA expression for $\tilde{\beta}$ indicates that since $k_f/k_i \approx 1$ (e.g. $\sim 0.6$ at $p_{lab} \approx$ 1500 MeV/$c$ for either of the $\bar{p}p \to \pi^-\pi^+$ and $\bar{p}p \to K^-K^+$ reactions), $A_{0n} \sim 1$ will result as in the last section, provided $c_0 \sim i$ and $c_1 \sim 1$. We shall see below (in a

DWBA-type calculation) that empirically favored values of $c_0$ and $c_1$ are indeed rather close to $c_0 = i$ and $c_1 = 1$, which lead to a $\tilde{\beta}$ that is almost angle-independent. We emphasize that in order to obtain $A_{0n} \approx 1$, it is essential that either $\tilde{V}_r$ or $\tilde{V}_p$ has an imaginary part so that Im $c(q) \neq 0$.

In order to evaluate reasonable reaction amplitudes in eqs. (25) and (26), it is necessary to include the effects due to the initial $\bar{p}p$ distorted wave. In the present exploratory study the $\bar{p}p$ optical potential is assumed to have a simple form [17])

$$V_{\rm opt}^{\rm el} = V^C + iW^C + V^{LS}(\boldsymbol{L}\cdot\boldsymbol{S}) \tag{39}$$

with

$$V^C = V_0 \Big/ \left[1+\exp\left(\frac{r-R^C}{a^C}\right)\right], \tag{40}$$

$$W^C = W_0 \Big/ \left[1+\exp\left(\frac{r-R'^C}{a'^C}\right)\right], \tag{41}$$

$$V^{LS} = -V_0^{LS}\frac{1}{a^{LS}r}\exp\left(\frac{r-R^{LS}}{a^{LS}}\right)\Big/\left[1+\exp\left(\frac{r-R^{LS}}{a^{LS}}\right)\right]^2. \tag{42}$$

The parameters of this optical potential are adjusted so as to reproduce the observed $\bar{p}p$ elastic cross section $d\sigma/d\Omega$ and polarization $P$. Again, reflecting the semi-quantitative nature of this study, only an approximate optimization of these parameters is attempted. The favored values of the $\bar{p}p$ optical potential parameters are listed in table 2 (case A), and the corresponding fits to the data are shown in figs. 3a and 3b. One can see from these figures that both $d\sigma/d\Omega$ and $P$ for $\bar{p}p$ elastic scattering are reproduced reasonably well. For the sake of a later discussion, we also consider a case that is devoid of the surface $LS$ term in eq. (39). Since in this case $P$ for $\bar{p}p$ elastic scattering is identically zero, we use only the cross-section data as input to determine the optical-potential parameters. The favored values of

TABLE 2

Parameters in the $\bar{p}p$ optical potential. $V_0$ and $W_0$ are given in fm$^{-1}$, and $R$ and $a$ in fm. Parameter set A includes both the central and surface $LS$ terms in the optical potential eq. (39), and is adjusted to reproduce the observed $d\sigma/d\Omega$ and the polarization $P$ for $\bar{p}p$ elastic scattering. Parameter set B contains only the central term, which is fitted to the $d\sigma/d\Omega$ for the $\bar{p}p$ elastic scattering. The entries in parentheses are parameters held fixed in fitting the data

| | $V_0$ | $R^C$ | $a^C$ | $W_0$ | $R'^C$ | $a'^C$ | $V_0^{LS}$ | $R^{LS}$ | $a^{LS}$ |
|---|---|---|---|---|---|---|---|---|---|
| $p_{\rm lab} = 1550$ MeV/$c$ | | | | | | | | | |
| A | −0.260 | 1.47 | (0.001) | −0.188 | 1.25 | (0.001) | 0.0382 | 1.22 | 0.012 |
| B | −0.287 | 1.18 | (0.001) | −0.377 | 1.42 | (0.001) | (0) | - | - |
| $p_{\rm lab} = 988$ MeV/$c$ | | | | | | | | | |
| A | −0.266 | 1.44 | 0.14 | −0.137 | 1.20 | (0.001) | 0.0386 | 1.43 | 0.002 |
| B | −0.309 | 1.30 | 0.035 | −0.189 | 1.60 | (0.001) | (0) | - | - |

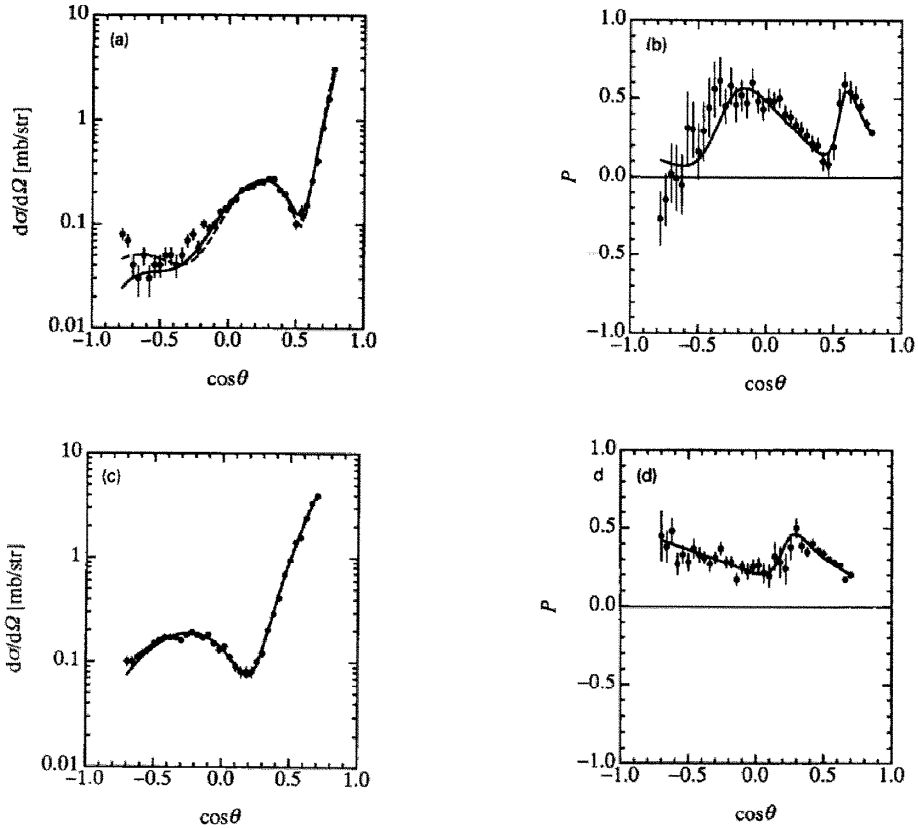


Fig. 3. Differential cross sections ($d\sigma/d\Omega$) and polarizations ($P$) of the elastic $\bar{p}p$ reaction: (a) $d\sigma/d\Omega$ and (b) $P$ at $p_{lab} = 1550$ MeV/$c$; (c) $d\sigma/d\Omega$ and (d) $P$ at $p_{lab} = 988$ MeV/$c$. In figs. 3a and 3c, the solid (dashed) line corresponds to case A (B) explained in table 2. In figs. 3b and 3d, the results for case A (the only relevant case) are shown. The data are taken from Kunne *et al.* [18]).

the parameters are given as case B in table 2, and the corresponding results for $d\sigma/d\Omega$ are shown in figs. 3a and 3c.

We consider the $\bar{p}p \to K^-K^+$ and $\bar{p}p \to \pi^-\pi^+$ reactions at the highest LEAR energy, $p_{lab} = 1550$ MeV/$c$. Since the validity of the diffraction model in the previous section is expected to be better at higher incident energies, we shall compare the results of the DWBA-type calculation to those of the diffraction model at $p_{lab} = 1550$ MeV/$c$. In addition, in view of the fact that for $\bar{p}p \to K^-K^+$ the maximal asymmetry phenomenon is seen even at such a low momentum as $p_{lab} = 988$ MeV/$c$, we will also present our results for $\bar{p}p \to K^-K^+$ at $p_{lab} = 988$ MeV/$c$. This example will also serve to illustrate the energy dependence of the present DWBA-type calculation. The parameters appearing in eqs. (32), (34) and (35) are determined by fitting the experimental $d\sigma/d\Omega$ and $A_{0n}$. Again, we have not performed a complete parameter search but rather have contented ourselves with a semi-quantitative fit to the data.

The favored values of the parameters are summarized in table 3. To avoid a plethora of parameters, we have kept some of these parameters unchanged; these fixed parameters are parenthesized in table 3.

We first discuss the numerical results of the $\bar{p}p \to K^- K^+$ reaction. In order to examine the role of the $LS$ term of the initial $\bar{p}p$ optical potential in explaining the observed $A_{0n}$, we compare the two different cases given in table 3. In table 3, "AK" ("BK") corresponds to the use of the initial $\bar{p}p$ optical potential case A (case B) of table 2. Thus the cases labeled "AK" ("BK") include (exclude) the $LS$ term in the $\bar{p}p$ optical potential. Within our semi-quantitative parameter searches, we could not determine the transition potentials uniquely, as exemplified by cases AK and AK1 in table 3. In these two cases the imaginary parts of the short-range term of $V_r$ have an equal magnitude but opposite signs, and yet both cases give almost identical observables so long as $\tilde{V}_p$ is given by eq. (34). Despite this nonuniqueness, we can still point out a number of features that characterize the favored form of $\Gamma$ in our fit. We find that $\Gamma$ must involve a sum of short- and long-ranged contributions in order to reproduce the $d\sigma/d\Omega$ and $A_{0n}$ data. Moreover, both $V_r$ and $V_p$ must contain an imaginary component acting at short distances (see fig. 4), which may be interpreted as representing the final-state interaction.

Figs. 5 and 6 show $d\sigma/d\Omega$ and $A_{0n}$ for $\bar{p}p \to K^- K^+$ calculated with the effective transition operators listed in table 3: AK (solid line) and BK (dashed line). For the sake of comparison, we also show the results (dotted line) obtained using a plane-wave initial state (PWBA) together with the effective transition operator of case AK. As can be seen from figs. 5a and 5b, the precise form of the initial-state distortion hardly matters. In particular, the inclusion of the $LS$ term in the initial $\bar{N}N$ optical potential leads to no significant difference in the calculated $d\sigma/d\Omega$ or $A_{0n}$; both

TABLE 3

Parameters in $V_r$ and in $c(q)$ that specify the effective transition operator $\Gamma$ for the $\bar{p}p \to M^- M^+$ reactions. See eqs. (32) and (34). $V_i$'s are given in $fm^{-2}$, $a_i$'s and $R_i$'s in fm, and the angles $\theta_i$ and $\phi_i$ in radians. For explanations on the different cases, AK, AK1, BK, AP and BP, see the text. The entries in parentheses are parameters held fixed in fitting the data

| | $V_1$ | $\theta_1$ | $a_1$ | $R_1$ | $V_2$ | $\theta_2$ | $a_2$ | $R_2$ | $\lvert c_0\rvert$ | $\phi_0$ | $\lvert c_1\rvert$ | $\phi_1$ |
|---|---|---|---|---|---|---|---|---|---|---|---|---|
| $\bar{p}p \to K^- K^+$; $p_{lab} = 1550$ MeV/$c$ | | | | | | | | | | | | |
| AK | −129 | −1.13 | (0.1) | (0) | 0.101 | (0) | 0.57 | (0) | 1.32 | $\frac{1}{2}\pi$ | 0.90 | (0) |
| AK1 | −129 | 1.13 | (0.1) | (0) | 0.101 | (0) | 0.57 | (0) | 1.32 | $\frac{1}{2}\pi$ | 0.89 | (0) |
| BK | −128 | −1.51 | (0.1) | (0) | 0.064 | (0) | 0.62 | (0) | 1.66 | $\frac{1}{2}\pi$ | 0.92 | (0) |
| $p_{lab} = 988$ MeV/$c$ | | | | | | | | | | | | |
| AK | 475 | −0.15 | (0.1) | (0) | −5.91 | (0) | 0.27 | (0) | 1.70 | −0.62 | −1.70 | −1.20 |
| BK | 506 | −0.18 | (0.1) | (0) | −6.12 | (0) | 0.27 | (0) | 1.55 | −0.51 | −1.43 | −1.21 |
| $\bar{p}p \to \pi^- \pi^+$; $p_{lab} = 1550$ MeV/$c$ | | | | | | | | | | | | |
| AP | −413 | −1.32 | (0.1) | (0) | −0.16 | 1.38 | (0.05) | 1.38 | −1.46 | −0.83 | 1.25 | (0) |
| BP | −507 | −1.48 | (0.1) | (0) | −0.18 | 1.40 | (0.05) | 1.40 | −1.32 | −0.86 | 1.21 | (0) |

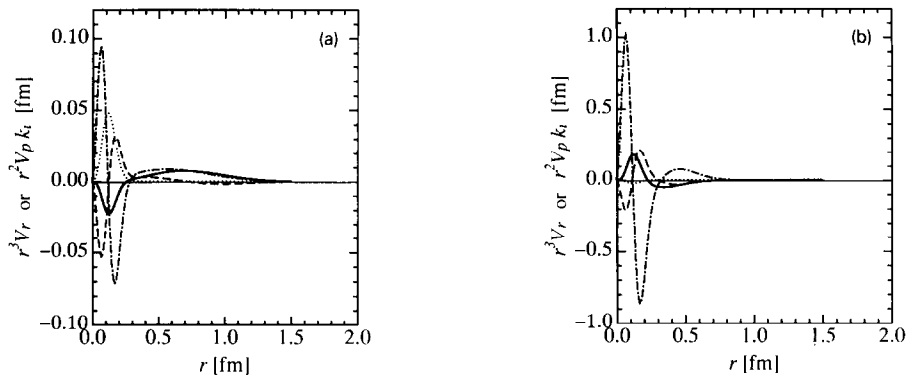


Fig. 4. The radial dependence of $r^3V_t(r)$ and $r^2V_p(r)k_t$, eqs. (34) and (32), for the $\bar{p}p \to K^-K^+$ reaction. Of the various cases shown in table 3, (a) represents case AK at $p_{lab} = 1550$ MeV/$c$ and (b) represents case AK at $p_{lab} = 988$ MeV/$c$. The solid (dotted) line is the real (imaginary) part of $r^3V_r$; the dashed (dash-dotted) line is the real (imaginary) part of $r^2V_pk_t$.

cases can explain the observed large values for $A_{0n}$. This insensitivity to the initial $LS$ distortion is also seen in table 3, where parameter set BK, a case devoid of initial $\bar{p}p$ $LS$ distortion, is remarkably close to parameter set AK. We therefore conclude that the $LS$ term in the initial $\bar{N}N$ distortion is not crucial in giving rise to large values of $A_{0n}$ for the $\bar{p}p \to K^-K^+$ reaction. A similar conclusion could be obtained by considering the underlying physical processes suggested by the favored values of the transition potential parameters. According to table 3, the effective range of $\Gamma$ needed to fit the $A_{0n}$ data is much smaller than that of the $LS$ term in

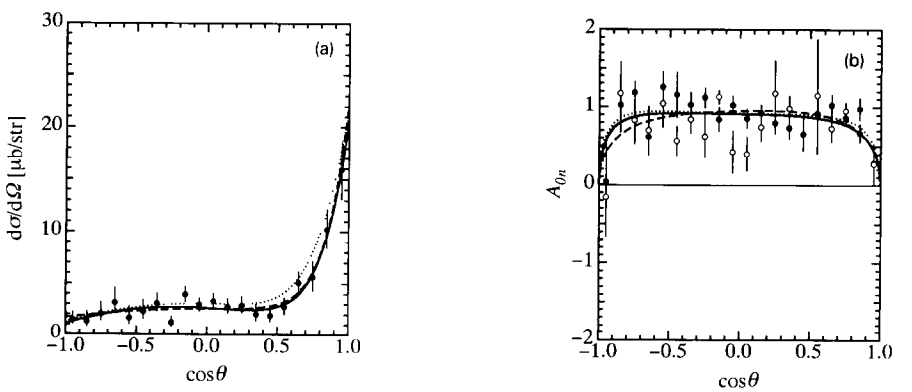


Fig. 5. Differential cross sections (a) and asymmetries (b) for the $\bar{p}p \to K^-K^+$ reaction at $p_{lab} = 1550$ MeV/$c$ calculated in the DWBA-type approach. The solid line corresponds to the result of case AK of table. 3. The dashed line represents case BK with no initial $\bar{p}p$ LS distortion (see text), and the dotted line is given by the transition potential AK with the initial $\bar{p}p$ state taken to be a plane-wave (PWBA). The data points in fig. (a) are $d\sigma/d\Omega$ at $p_{lab} = 1.60$ GeV/$c$ taken from Eisenhandler *et al.* [1]). The data points in fig. (b) are $A_{0n}$ at $p_{lab} = 1.5$ GeV/$c$ (○) taken from Birsa *et al.* [3]) and $A_{0n}$ at $p_{lab} = 1.6$ GeV/$c$ (●) taken from Carter *et al.* [2]).

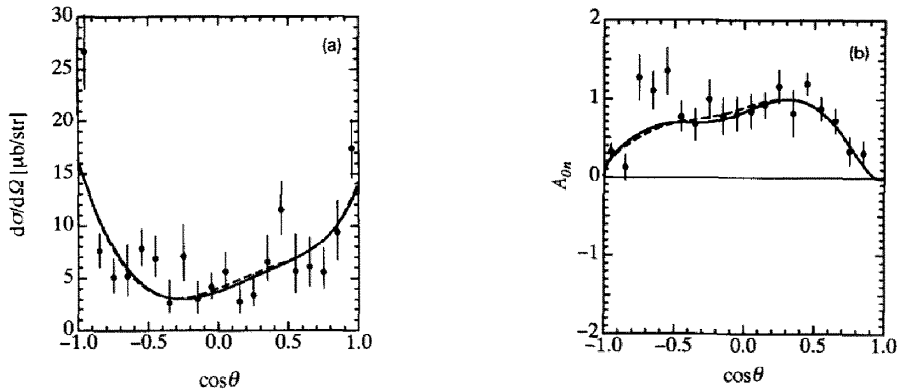


Fig. 6. Differential cross sections $d\sigma/d\Omega$ (a), and asymmetries $A_{0n}$ (b) for the $\bar{p}p \to K^- K^+$ reaction at $p_{lab} = 988$ MeV/$c$ calculated in a DWBA-type approach. The solid line corresponds to the result of case AK listed in table 3, while the dashed line represents case BK with no initial $\bar{p}p$ LS distortion (see text). The data points in (a) are $d\sigma/d\Omega$ at $p_{lab} = 0.99$ GeV/$c$ taken from Eisenhandler *et al.* [1]). The data points in (b) are $A_{0n}$ at $p_{lab} = 1.0$ GeV/$c$ taken from Birsa *et al.* [3]).

the initial $\bar{N}N$ optical potential ($\sim$1.2 fm, see table 2). Thus the annihilation reaction in question originates from a very central $\bar{p}p$ interaction region (well inside the periphery where the effective initial $\bar{N}N$ *LS* interaction acts) and consequently $A_{0n}$ for this annihilation reaction is not affected by the *LS* term in the $\bar{p}p$ optical potential.

We next discuss the $\bar{p}p \to \pi^- \pi^+$ reaction. The favored values of the parameters in the transition potentials $V_p$ and $V_r$ for this reaction are also shown in table 3. The radial behavior of the transition potentials is depicted in fig. 7, and the $d\sigma/d\Omega$ and $A_{0n}$ calculated with these transition potentials are shown in fig. 8. The quality of agreement of the calculated observables with data is less impressive for this

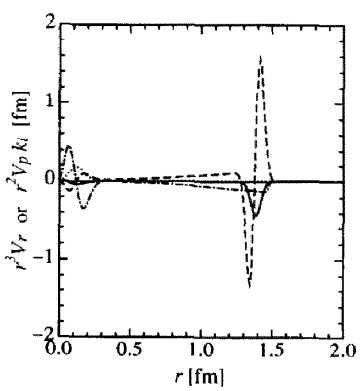


Fig. 7. The radial dependence of $r^2 V_r(r) r$ and $r^2 V_p(r) k$, for the $\bar{p}p \to \pi^- \pi^+$ reaction at $p_{lab} = 1550$ MeV/$c$, corresponding to case AP in table 3. The solid (dotted) line is the real (imaginary) part of $r^2 V_r r$; the dashed (dash-dotted) line is the real (imaginary) part of $r^2 V_p k_i$.

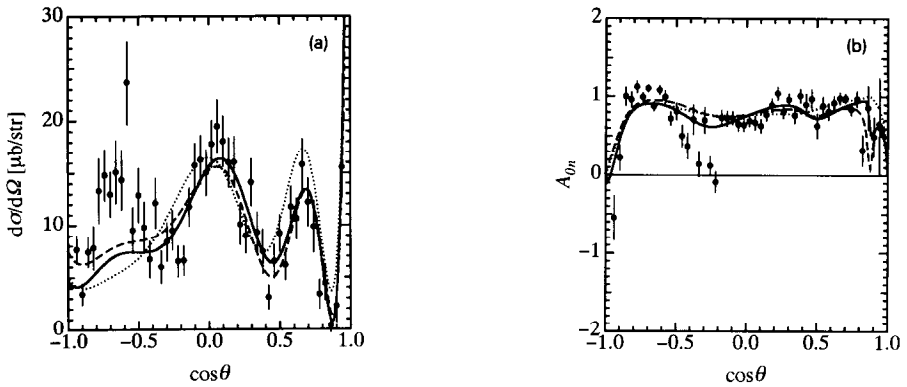


Fig. 8. Differential cross sections (a) and asymmetries (b) for the $\bar{p}p \to \pi^-\pi^+$ reaction at $p_{lab} = 1550$ MeV/$c$ calculated in the DWBA-type approach. The solid line corresponds to case AP of table 3. The dashed line represents case BP with no initial $\bar{p}p$ *LS* distortion, while the dotted line is given by the transition potential AK with initial plane-wave (PWBA). The data points are for $p_{lab} = 1.60$ GeV/$c$ and taken from ref. [1]) (fig. 9a) and ref. [2]) (fig. 9b).

reaction than for the $\bar{p}p \to K^-K^+$ case. As in the $\bar{p}p \to K^-K^+$ case, the results of the PWBA calculation are remarkably close to the DWBA results in the $\bar{p}p \to \pi^-\pi^+$ reaction.

To reproduce the observed angular oscillations in $d\sigma/d\Omega$, the transition potentials are required to be strongly peaked around $R \sim 1.4$ fm. The strong peak shown in fig. 7 is likely to be an artifact of the short range ($1.2 \sim 1.5$ fm) used in the initial $\bar{N}N$ Woods-Saxon-like potential, eq. (44). This range is much shorter than what is expected from the more realistic meson-exchange $\bar{N}N$ potential. One expects that the long-range attraction of the meson-exchange potential pulls the $\bar{N}N$ wave function into the annihilation region, thereby effectively increasing the range of the more central annihilation process. Our simple $\bar{N}N$ potential fails to simulate this feature, as can be seen in table 2 (compare $R^C$ and $R'^C$). Since the reaction $\bar{p}p \to \pi^-\pi^+$ is more sensitive to peripheral interactions than the $\bar{p}p \to K^-K^+$ reaction, we should have used a more realistic initial-state distortion potential in fitting the $\bar{p}p \to \pi^-\pi^+$ data. Unfortunately, the shape of the potential for the $\bar{p}p$ elastic scattering cannot be uniquely determined as seen from the fact that even our simple Woods-Saxon potential can reproduce both of the cross section and polarization. Though it might be possible to choose a different potential for the elastic scattering by using the two-meson production data, that is beyond the scope of the present exploratory study.

The limited success of the present DWBA-type calculation for the $\bar{p}p \to \pi^-\pi^+$ observables notwithstanding, we may still make the following observation: in order to reproduce the $\bar{p}p \to \pi^-\pi^+$ data to the extent achieved in fig. 8, the effective transition operator $\Gamma$ for $\bar{p}p \to \pi^-\pi^+$ must act at much larger distances than the $\Gamma$ for $\bar{p}p \to K^-K^+$ (compare fig. 7 with fig. 4). This finding is consistent with our earlier argument (sect. 2) that the $\bar{p}p \to K^-K^+$ reaction seems to originate from a more central collision than the $\bar{p}p \to \pi^-\pi^+$ reaction. We emphasize once again that the

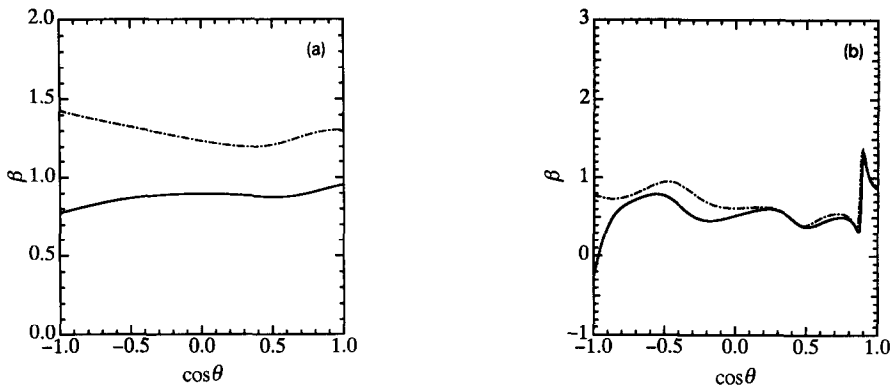


Fig. 9. The function $\tilde{\beta}$ of eq. (24) at $p_{\rm lab} = 1550$ MeV/$c$ calculated with (a) the parameter set AK for the $\bar{p}p \to K^-K^+$ reaction and (b) the parameter set AP for the $\bar{p}p \to \pi^-\pi^+$ reaction. The solid lines represent Im $\tilde{\beta}$, while the dashed lines give $|\tilde{\beta}|$.

use of more complicated effective transition potentials would not modify the essential features of the results obtained here; the smooth behavior of $A_{0n}$ would persist provided eq. (34) holds.

Finally, to make connection with the schematic models described in sect. 2, we present in fig. 9 the angular behavior of $\tilde{\beta}$ calculated with the effective transition operator of eqs. (32) and (34). Fig. 9 indicates that for the $\bar{p}p \to K^-K^+$ reaction at $p_{\rm lab} \approx 1.5$ GeV/$c$, where the extraordinary behavior of $A_{0n}$ is particularly prominent, $\tilde{\beta}$ is a very smooth function of cos $\theta$. Also for the $\bar{p}p \to \pi^-\pi^+$ reaction, $\tilde{\beta}$ is far smoother than one would expect from its oscillating cross section. Furthermore, $\tilde{\beta} \approx i$, and $|\tilde{\beta}|$ is rather close to 1. This implies that $A_{0n} \approx 1$ according to eq. (30). These features lend some support to the assumption made in our schematic analysis of sect. 2.

## 4. Summary and conclusions

This study was motivated by the extraordinary behavior of $A_{0n}$ observed for the $\bar{p}p \to \pi^-\pi^+$ and $\bar{p}p \to K^-K^+$ reactions; the measured values of $A_{0n}$'s are surprisingly large over a wide angular range and nearly independent of $p_{\rm lab}$ for the higher LEAR energies. This highly noteworthy feature seemed to call for a simple explanation. We have examined some schematic models based on a simple relation eq. (5) between helicity-flip and nonflip partial-wave amplitudes. Our illustrative models suggest the possibility that this extremely simple relation may be at least partly responsible for the observed remarkable behavior of $A_{0n}$. The basic ansatz, eq. (5), is motivated by the expectation that the helicity-flip amplitude would be most effective at the interaction surface where there is the least "absorption" (meaning the least loss of flux from the final two-meson channel). Although it is obviously desirable to examine under what circumstances eq. (5) is reasonable, we have

basically relegated this question to future studies and have mostly concentrated on the consequences of the relation eq. (5).

However, in order to obtain a better understanding of the reaction mechanism, we have also carried out a simple DWBA-type calculation. A full-fledged DWBA calculation is not possible (and probably not warranted) at present. One of the principal difficulties with such calculations is that the final-state meson-meson interactions are only poorly known at these high energies. Secondly, it may not be possible to separate the $\bar{N}N \to \bar{M}M$ transition interaction from that of the final-state interactions, since perturbation theory is not applicable at these energies. This has obliged us to use an effective transition operator $\Gamma$ which simulates the combined effects of the final-state interaction and the transition operator. The initial-state interaction is simulated by an $\bar{N}N$ optical potential. The most important aspect of the initial $\bar{N}N$-channel interaction seems to be the strong $\bar{N}N$ absorption in the low impact-parameter region. This implies that the low elastic $\bar{N}N$ partial-wave amplitudes would be close to their unitarity limit. We have considered this aspect in our parameter search in the present DWBA-type analyses.

The results obtained in the DWBA-type approach indicate: (i) The strongly angular-dependent cross section and the smooth asymmetry can be reproduced simultaneously with the use of simple transition potentials parameterized as in eqs. (32), (34) and (35). (ii) The transition potentials that have been approximately optimized to reproduce the data, result in a behavior of the parameter $\tilde{\beta}$ (see fig. 9) consistent with the basic ansatz, eq. (5), used in our schematic models. (iii) The initial distortion due to the $\bar{N}N$ potential plays a minor role in explaining the observed behavior of $A_{0n}$. (iv) It seems necessary that $\Gamma$ for the $\bar{p}p \to M^- M^+$ reaction contains a sum of at least two terms with different ranges. This feature could be anticipated in the case of $\bar{p}p \to K^- K^+$ from the two-slope angular structure in the measured $d\sigma/d\Omega$, and in the case of $\bar{p}p \to \pi^- \pi^+$ from the pronounced forward peaking in $d\sigma/d\Omega$ followed by angular oscillation. (v) The interference term arising from the sum of the two transition potentials, $V_r$ and $V_p$ (which also mimic the final-state interactions), is essential to yield large asymmetries. We may mention *en passant* that this feature is similar to what has been found at low energies ($p_{\text{lab}} \lesssim 1$ GeV/$c$) [ref. [6])]. Finally (vi) the $\bar{p}p \to K^- K^+$ reaction takes place at much shorter distances than the $\bar{p}p \to \pi^- \pi^+$ reaction. This result lends support to the argument based on an analogy to QED [15]) that the larger the number of initial $\bar{q}q$ valence pairs which need to be annihilated for a specific $\bar{N}N$ annihilation reaction to occur, the more central is the reaction.

Since our explanation of the maximal $A_{0n}$ is based on a rather general picture, we may expect that the maximal $Z_{0n}$ will persist as the incident energy increases. This is in contrast to the resonance analysis [8]), which assumes the dominance of one partial wave at each energy, an assumption which in all likelihood fails badly at higher energies. However, as argued by Carlson *et al.* [19]), when the perturbative QCD regime is reached (probably at the SuperLEAR or KAON energies), our

hadronic description will break down and should be replaced by a perturbative QCD description (suitably adapted to these exclusive hadronic reactions). An interesting question is whether the onset of the perturbative QCD regime can be observed in $A_{0n}$. The large asymmetry would disappear were the short-distance QCD arguments valid [see Brodsky [20]) as well as reviews by Mueller [21]) and by Chernyak and Zhitnitsky [22])]. However, finite asymmetries might be observed even at high energies and high momentum transfers if, as emphasized by Landshoff [23]), the perturbative QCD processes involving independent qq scatterings are important in the exclusive hadronic reactions. There, the asymmetries may exhibit a very characteristic oscillation as a function of the incident energy for a fixed large scattering angle [19]). In either case the behavior of $A_{0n}$ may serve as a signal for the onset of the perturbative QCD regime. Thus, the measurement of $A_{0n}$ of the $\bar{p}p \to \pi^- \pi^+$ and $\bar{p}p \to K^- K^+$ reactions at the SuperLEAR and KAON energies will be extremely useful not only for a better understanding of the nature of the extraordinarily large asymmetry observed in the LEAR energy region, but also for monitoring the possible onset of perturbative QCD and its mechanism in exclusive hadronic reactions.

The initial thinking about the physical picture presented here was influenced by a private communication from D. Bugg to one of the authors (FM). After completion of this work we have learned that the final experimental data of ref. [3]) was published [24]). The gross features discussed in our present work have been confirmed by the new data. This work is supported in part by National Science Foundation Grant No. PHYS-9006844.

## References

1) E. Eisenhandler *et al.*, Nucl. Phys. **B96** (1975) 109
2) A.A. Carter *et al.*, Nucl. Phys. **B127** (1977) 202
3) R. Birsa *et al.*, Nucl. Phys. **B** (Proc. Suppl.) **8** (1989) 141
4) T. Tanimori *et al.*, Phys. Rev. **D41** (1990) 744 and references therein
5) G.Q. Liu and F. Tabakin, Phys. Rev. **C41** (1990) 665
6) V. Mull, K. Holinde and J. Speth, Phys. Lett. **B275** (1992) 12
7) S. Mundigl, M. Vicente Vacas and W. Weise, Nucl. Phys. **A523** (1991) 499
8) A.A. Carter *et al.*, Phys. Lett. **B67** (1977) 117;
A.A. Carter, Phys. Lett. **B67** (1977) 122
9) A.D. Martin and M.R. Pennington, Phys. Lett. **B86** (1979) 93
10) B.R. Martin and D. Morgan, Nucl. Phys. **B176** (1980) 355;
B.R. Martin and G.C. Oades, Nucl. Phys. **A483** (1988) 669
11) B.R. Martin and G.C. Oades, Nucl. Phys. **A483** (1988) 669; Contributed paper V-2, The PANIC XII Conference, ed. T.W. Donnelly (MIT, 1990);
N. Isgur and K. Königsmann, Nucl. Phys. **A527** (1991) 491c
12) S. Godfrey and N. Isgur, Phys. Rev. **D32** (1985) 189;
T.H. Burnett and S.R. Sharpe, Ann. Rev. Nucl. Part. Sci. **40** (1990) 327
13) S. Takeuchi, F. Myhrer and K. Kubodera, AIP Conf. Proc. **243** (1992) 358

14) S. Takeuchi, F. Myhrer and K. Kubodera, Inst. Phys. Conf. Ser. **124** (1992) 303; Workshop on Physics at SuperLEAR (eds. C. Amsler and D. Urner) Zürich, October (1991)
15) J. Carbonell *et al.*, Z. Phys. **A334** (1989) 329
16) H. Høgaasen, Phys. Norvegica **5** (1971) 219;
H. Høgaasen and C. Michael, Nucl. Phys. **B44** (1972) 214;
V. Barger and R.J.N. Phillips, Nucl. Phys. **B87** (1975) 221
17) E. Eisenhandler *et al.*, Nucl. Phys. **B113** (1976) 1
18) R.A. Kunne *et al.*, Nucl. Phys. **B323** (1989) 1
19) C.E. Carlson, M. Chachkhunashvili and F. Myhrer, Phys. Rev. **D46** (1992) 2891
20) S.J. Brodsky and G.P. Lepage, Phys. Rev. **D22** (1980) 2848;
S. Brodsky, in Proc. Workshop on nuclear chromodynamics, eds. S. Brodsky and E. Moniz (World Scientific, Singapore, 1991) p. 3
21) A.H. Mueller, Phys. Reports **73** (1981) 237
22) V.L. Chernyak and A.R. Zhitnitsky, Phys. Reports **112** (1984) 173
23) P.V. Landshoff, Phys. Rev. **D10** (1974) 1024;
P. Cvitanoic, Phys. Rev. **D10** (1974) 338
24) A. Hasan *et al.*, Nucl. Phys. **B378** (1992) 3